Chapter 11

Silicon isotopic fractionation during $H_4SiO_4^0$ adsorption onto iron oxides in basaltic ash soils differing in weathering stage *

Abstract

The sequestration of silicon in soil clay-sized iron oxides may affect the terrestrial cycle of Si. Iron oxides indeed specifically adsorb aqueous monosilicic acid ($H_4SiO_4^0$), thereby influencing Si concentration in soil solution, and hence in waters drained from watersheds. Here we study the impact of $H_4SiO_4^0$ adsorption on the fractionation of Si isotopes in basaltic ash soils differing in weathering stage, hence in clay and Fe-oxide contents. Adsorption was measured in batch experiment series designed as function of time (0-72 h) and initial concentration (ic) of Si in solution (0.61-1.18 mM) at 20°C, constant pH (5.5) and ionic force (1 mM). After various soil-solution contact times, the δ^{30}Si vs. NBS28 compositions were determined in selected solutions by MC-ICP-MS Nu Plasma in medium resolution, operating in dry plasma with Mg doping with an average precision of ± 0.15‰ (± $2\sigma_{SEM}$).

*Article in preparation: Opfergelt et al.
Complementary calculation in Appendix F.

The quantitative adsorption of $H_4SiO_4^0$ by soil Fe-oxides left a solution depleted in light Si isotopes, which confirms previous study on synthetic Fe-oxides. Measured against its initial composition ($\delta^{30}Si = +0.02 \pm 0.07‰$ ($\pm 2\sigma_{SD}$)), the solutions were systematically enriched in ^{30}Si reaching maximum $\delta^{30}Si$ values ranging between +0.16 ‰ and +0.95 ‰ after 72h contact time. The enrichment of the solution in heavy isotopes increased with increasing values of three parameters: soil weathering stage, iron oxide content, and proportion of short-range ordered Fe-oxide. The Si isotopic signature of the solution was partly influenced by simultaneous processes of Si release, likely through mineral dissolution and Si desorption from oxide surfaces, depending on soil type. Our data imply that in natural environments, $H_4SiO_4^0$ adsorption by soil Fe-oxides impacts the Si isotopic signature of the soil solution exported to water streams.

11.1 Introduction

Silicon released as monosilicic acid ($H_4SiO_4^0$) by mineral weathering is a major solute in continental surface and ground waters (Gaillardet et al., 1999). In soils, the concentration of aqueous $H_4SiO_4^0$ is ruled by Si uptake by plants, silicate dissolution, formation of silicate minerals, and Si adsorption onto secondary oxides (McKeague and Cline, 1963c). Al and Fe-oxides specifically adsorb $H_4SiO_4^0$ (Beckwith and Reeve, 1963; Jones and Handreck, 1963; McKeague and Cline, 1963bc). $H_4SiO_4^0$ interacts with Fe-oxide surface OH groups through ligand exchange to form silicate bi-dendate innersphere complex (Hiemstra et al., 2007; Parfitt, 1978; Pokrovski et al., 2003). Following adsorption, Si can be incorporated into the Fe-oxide particle (Carlson and Schwertmann, 1981). Surface Si polymerization may also occur (Hiemstra et al., 2007; Swedlund and Webster, 1999). The sequestration of Si in soil clay-sized Fe-oxides can thus affect the Si terrestrial cycle by influencing Si concentration in solution, and hence in waters drained from watersheds.

The influence of $H_4SiO_4^0$ adsorption by soil Fe-oxides upon the Si continental cycle is, however, poorly quantified as compared to other Si land reservoirs. Silicon isotopes can be used to trace this process. As compared to crustal rocks (Douthitt, 1982), river waters are depleted in ^{28}Si (Alleman et al., 2005; De La Rocha et al., 2000; Ding et al., 2004; Georg et al., 2006a 2007c), implying the existence of Si reservoirs enriched in ^{28}Si. Silicon uptake by biota favors the absorption of ^{28}Si in plants (Ding et al. (2005b 2008); Douthitt (1982); Opfergelt et al. (2006ab); Ziegler et al. (2005a); Chapter 7; Chapter

8; Appendix C), diatoms (Alleman et al., 2005; Cardinal et al., 2005; De La Rocha et al., 1997) and sponges (De La Rocha, 2003). Soil clay-sized components sequestrate light Si isotopes (Georg et al. (2006a); Ziegler et al. (2005ab); Chapter 8). Two processes may induce this sequestration: the formation of secondary silicate minerals (Ziegler et al., 2005b), and the specific adsorption of $H_4SiO_4^0$ onto secondary oxides, both short range-ordered (sro) and crystalline, as shown for synthetic ferrihydrite (sro) and goethite (crystalline) (Chapter 10). Rock weathering and soil development lead to the formation of both clay minerals and secondary oxides. With increasing weathering in well drained conditions, Fe-oxide content increases, but the nature of oxides may change. In volcanic ash soils, sro Fe-oxides dominate the oxide pool in least weathered soils, whereas crystalline Fe-oxides are largely dominant, if not exclusive, in most weathered soils (e.g. Delvaux et al. (1989)).

Here, we report on the Si isotopic fractionation induced by $H_4SiO_4^0$ adsorption onto Fe-oxide in soils. The experiments were designed to answer two questions of natural significance: (1) Does Si isotope fractionation occur during Si adsorption onto soil Fe-oxide without any prior cleaning up of oxide surface? (2) How does this fractionation vary with soil weathering stage, content of soil Fe-oxide, and relative proportion of sro and crystalline Fe-oxide? For these purposes, we use soils derived from similar basaltic ash, but differing in weathering stage, thus showing variable Fe-oxide contents and contrasted proportions of sro and crystalline Fe-oxide. Our study involves the prior characterization of soil materials and the quantitative determination of $H_4SiO_4^0$ adsorption in controlled conditions of temperature, solid:liquid ratio, pH and ionic force.

11.2 Materials and methods

11.2.1 Environmental framework and major soil mineral components

The study areas are located in Cameroon, West Africa: (1) the Mungo plain (60-350m asl; axis Njombé-Penja-Loum, 4°30'-4°53'N 9°37'-9°50'E, 70km north of Douala), (2) the low Eastern slopes of Mt Cameroon volcano (alt. 4095m) (400-900m asl; 4°09'-4°13'N 9°16'-9°21'E). These areas will be referred to as Mungo and Mt Cameroon respectively. The climate is humid tropical with a rainy season extending from March to November. The mean annual rainfall ranges between 2500 and 2800 mm $year^{-1}$ in Mungo, and between 2250 and 2800 mm $year^{-1}$ in Mt

Cameroon area. The mean annual temperature varies between 22.4°C (870m asl) and 27.5°C (60m).

The Mungo plain is a graben located between the stratovolcanoes Mt Cameroon and Mt Manengouba (Nkouathio et al., 2002), part of the N30°E Cameroon Hot Line (Déruelle et al., 2007). In Mungo, the soils derive from basaltic ash and pumice deposits. In the Mt Cameroon area, soils develop from fine basaltic pyroclasts transported by mudflows from the top of the volcano. All volcanic deposits are Quaternary in age. Soil weathering sequences correspond in both areas to the mineralogical sequence ash-allophane-halloysite-kaolinite (Delvaux, 1988; Delvaux et al., 1989 1990b; Sieffermann, 1973). With increasing weathering stage, the content of weatherable minerals decreases whereas clay and Fe-oxide contents increase (Delvaux et al., 1989; Sieffermann, 1973). Gibbsite and titanium-oxides constitute minor secondary phases. Fe-oxides are by far the dominant clay-sized secondary oxides. From previous studies based on TEM (Transmission Electron Microscopy) and selective dissolution (Sieffermann, 1973), as well as on TEM, selective dissolution, Mössbauer spectroscopy and ESR (Electron Spin Resonance) spectroscopy (Delvaux, 1988), available data converge to show that sro Fe-oxides (ferrihydrite) dominate the pool of Fe-oxide in the least weathered soils (Vitric Andosol; ISSS (1998)), whereas crystalline Fe-oxide (goethite) is largely dominant in the most weathered soils (Nitisol; ISSS (1998)). Selective dissolution allows estimating the respective pools of sro and crystalline Fe-oxides in these soils (Delvaux, 1988; Delvaux et al., 1989).

11.2.2 Soil and clay materials

Seven soil profiles were selected to cover a range of soils differing in weathering stage (WS). All soils were sampled under ancient banana cropping systems, and were thus long supplied with N-P-K fertilizers and carbonate amendments. Four soils were selected in Mungo (99-240 m asl), following increasing WS: Dia-Dia (DD), Sir (SR), Mbomé (MB) and Djungo (DJ), at the respective altitudes 204, 240, 99 and 163 m asl. Three soils were selected in Mt Cameroon area, following increasing WS: Molyko (MO), Ekona (EK), Mussaka (MU), at the respective altitudes 685, 613 and 545 m asl. Soil profiles were described and sampled according to FAO guidelines, bulk samples being collected from all horizons (00-110cm). The samples were air dried at room temperature during 24h and sieved at 2 mm to obtain the fine earth fraction (FEF<2mm). The clay fraction was recovered after sonication and dispersion with Na^+-saturated resins (Rouiller et al., 1972). Briefly, the

sand fraction (50-2000 μm) was separated through ultrasonic dispersion of FEF and repeated wet sieving. Clay and silt fractions (<50μm) were collected and submitted to prolonged dispersion with Na^+-resins. Clay (<2μm) was separated from silt by successive cycles of 24h decanting and pipetting. All experimental procedures were carried out on FEF and clay fractions, but analytical data, soil and clay properties were all expressed on a dry weight basis (constant weight after drying at 105°C).

11.2.3 Characterization of soil and clay properties

Soil pH was measured in deionised water (1g:5ml). The cation exchange capacity (CEC) of the FEF was determined by saturation by 1 M NH_4OAc, pH 7 (Page et al., 1982). Elemental analysis of the fine earth and clay fractions was carried out after loss on ignition at 950°C followed by borate fusion (Chao and Sanzolone, 1992). Briefly, a crushed sample of 100 mg was melted at 1000°C for 5 minutes in a graphite crucible in the presence of 0.4 g Li-tetraborate and 1.6 g Li-metaborate. The cooled melt was then dissolved in 100 ml of 2M HNO_3 under magnetic agitation at 90-100°C. Elemental contents were determined by Inductively Coupled Plasma - Atomic Emission Spectrometry (ICP-AES). The total contents of alkaline and alkaline-earth cations were summed up as the total reserve in bases (TRB), which estimates the content of weatherable minerals in mineral soil horizons (Herbillon, 1986). Dark oxalate (o) and dithionite-citrate-bicarbonate (DCB) extractable contents of Si, Al, Fe were determined on fine earth and clay fractions by well-known extraction procedures (o: Blakemore et al. (1981); DCB: Mehra and Jackson (1960)), and determination by ICP-AES.

11.2.4 Adsorption experiments

At all steps, acid-washed high density polyethylene (HDPE) ware and analytical grade *Pro Analysi* chemicals were used to minimise Si contamination.

Seven weathered AC, Bw and Bt horizons were selected at given depth (cm): DD (AC, 5-40), SR (Bw, 21-33), MB (AC, 5-32), DJ (Bw, 66-115), MO (Bw2, 60-92), EK (Bw1, 60-100), MU (Bt2, 65-110cm). The adsorption procedure followed the one described in Chapter 10. For the main experiment, the quantitative determination of $H_4SiO_4^0$ adsorption was done in controlled conditions of temperature (20°C), pH (5.5) and ionic force (1mM). We used a solid:liquid ratio at 1 g:20 ml to take into account the Fe-oxide content in soil materials as computed

on a Fe_2O_3 basis (<15%; Delvaux et al. (1989)). The experiments were carried out at two initial concentrations (ic) of Si in solution: 1.18 and 0.61 mMSi, and at 12, 24, 48 and 72h contact times. The FEF were in contact with the solutions through dialysis membrane (Spectrium Spectra/POR membrane, MWCO 12-14000). Experiment was done in duplicates: serie 1 was used to provide adsorption data and serie 2 was used for the determination of Si isotopes. Solution aliquots were collected at given contact times, acidified with suprapur HNO_3 and stored at 4°C in the dark, in acid-cleaned polypropylene bottles; Si concentration was determined by ICP-AES.

We carried out two additional adsorption experiments using the same procedure on, respectively, separate $SrCl_2$-washed and DCB-treated FEF samples at ic = 1.18 mM Si. The $SrCl_2$ washing involved four cycles of saturation-centrifugation by $SrCl_2$ 0.5M followed by washing by milliQ water. The DCB extraction was done according to Mehra and Jackson (1960). These treatments were aimed at, respectively, desorbing chloride-extractable $H_4SiO_4^0$ from oxide surfaces and extracting free iron oxide prior to the Si adsorption measurement.

11.2.5 Silicon isotopes analyses

The Si isotopic composition was measured in the solutions collected at each contact time for the main adsorption experiment. Dissolved Si from solution aliquots was (1) purified by triethylamine molybdate co-precipitation and combustion in covered Pt crucibles at 1000°C (De La Rocha et al., 1996), and (2) dissolved in dilute suprapur HF-HCl mixture (Cardinal et al., 2003).

The Si-isotopic compositions were measured using a Nu Plasma multicollector plasma source mass spectrometer (MC-ICP-MS) operating in dry plasma mode, with an external Mg doping to correct mass bias (Cardinal et al., 2003) and solving the isobaric interference of $^{14}N^{16}O$ on ^{30}Si (Abraham et al. (2008); Chapter 5). The analytical method was supported by an inter-laboratory comparison exercise and proved to be accurate on secondary reference materials (Reynolds et al. (2007); Chapter 6). To avoid matrix effects, the absence of major elements and Mo was controlled by ICP-AES before MC-ICP-MS analyses. Data were obtained by the sample-standard bracketing technique relative to the NBS28 silica sand standard (National Institute of Standard and Technology RM #8546) for silicon isotopes (Carignan et al., 2004) or in house standards ($pSiO_2$ or Quartz Merck) isotopically similar to NBS28 (Abraham et al. (2008); Chapter 5). In this study, our results were expressed as $\delta^{30}Si$ vs. NBS28 (‰) with an average precision and

accuracy below 0.15‰ ($\pm$ $2\sigma_{SEM}$) following:

$$\delta^{30}Si = \left[\frac{\left(\frac{^{30}Si}{^{28}Si}\right)_{\text{sample}}}{\left(\frac{^{30}Si}{^{28}Si}\right)_{\text{NBS28}}} - 1 \right] \times 1000$$

11.3 Results

11.3.1 Properties of soil and clay materials

Tables 11.1 and 11.2 present some major characteristics of FEF and clay fractions of the selected soils. They are strongly consistent with previous data (Delvaux et al., 1989; Sieffermann, 1973), with pH and CEC values ranging between 4.2 and 7.2, and 13 and 52 $cmol_c$ kg^{-1}, respectively. From the least to the most weathered soils, TRB, estimating the reserve of weatherable primary minerals, decreases from 712 to 43 $cmol_c$ kg^{-1} whereas clay content increases from 24 to 86%. The total iron content (Fe_t) of soil materials (86-180 g kg^{-1}) accords with the basaltic composition of parent ash (Sieffermann, 1973). There is a consensus about the interpretation of oxalate- and DCB-extractable Fe contents in soils (Borggaard, 1990; Cornell and Schwertmann, 1996; Schwertmann and Taylor, 1989; Shoji et al., 1993): oxalate generally extracts a pool involving sro Fe-oxide and humus-bound Fe (Fe_o) whereas DCB dissolves "free iron" (Fe_d), involving the Fe_o pool and crystalline Fe-oxides, thus excluding structural iron in silicates. The Fe_d/Fe_t ratio is thus used as a weathering index, whereas the Fe_o/Fe_d ratio reflects the relative proportion of sro Fe-oxide in the global pool of Fe-oxide. This interpretation is particularly valid in soils poor in humus-bound Fe, like the soils considered here (Delvaux et al., 1989).

Figures 11.1 and 11.2 illustrate how the selected materials (see section 11.2.4) are suited with respect to the objectives of the present study (see section 11.1). Indeed, soils exhibit contrasting degrees of weathering. Clay content is strongly and negatively correlated with TRB (r = -0.94), and positively with Fe_d/Fe_t ratio (r = 0.72) (Figure 11.1). In both sequences, DJ and MU soils are clearly set apart because of their very high clay content (85-86%). Figure 11.2 further shows the parallel increase of both clay and Fe_d contents in the FEF of selected materials, with Fe_d widely ranging from 23 to 82 g kg^{-1}. The range of Fe_d content is, however, wider in Mungo (23-82 g kg^{-1}) than in Mt Cameroon (35-58 g kg^{-1}) soil materials. As inferred from Figure 11.2(b), weathering and soil development have also a very strong impact on the nature of iron oxide in the clay-sized fractions of selected soil horizons:

Table 11.1: Major characteristics of the soil profiles (fine earth fraction <2mm): cationic exchange capacity (CEC), pH_{water}, Total Reserve in Bases (TRB), and particle size distribution (sand >50μm, silt 2-50μm, clay <2μm).

Prof.	Horiz.	Depth	CEC $cmol_c\ kg^{-1}$	pH_{H_2O}	TRB $cmol_c\ kg^{-1}$	Sand %	Silt %	Clay %
DD	Ap	0-5	22.3	7.14	703	61	14	25
DD	AC	5-40	21.5	6.80	712	61	15	24
SR	Ap1	0-5	35.2	7.18	469	20	39	42
SR	Bw	21-33	18.0	6.63	526	16	41	43
MB	Ap	0-5	52.6	7.52	323	27	27	58
MB	AC	5-32	29.4	6.75	438	25	38	37
DJ	Ap1	0-5	34.5	7.55	183	10	18	72
DJ	Bt	15-66	30.5	6.73	126	6	11	84
DJ	Bw	66-115	28.5	6.25	84	9	6	85
MO	Ap2	5-20	32.7	7.04	468	20	31	49
MO	Bw1	20-60	24.8	5.55	408	22	27	51
MO	Bw2	60-92	24.5	5.35	604	35	26	39
EK	Ap2	5-32	40.4	7.09	273	11	31	59
EK	Bt	32-60	25.7	6.60	252	10	27	64
EK	Bw1	60-100	30.5	5.63	321	13	30	56
MU	Ap2	5-25	13.6	4.37	63	4	24	72
MU	Bt1	25-65	21.7	4.23	43	3	14	83
MU	Bt2	65-110	20.4	4.44	48	2	12	86

crystalline Fe-oxides (goethite) largely dominate the Fe-oxide pool in the most weathered soils DJ and MU (Fe_o/Fe_d: 0.25-0.27) whereas sro Fe-oxides (ferrihydrite) dominate that pool in other soils (Fe_o/Fe_d: 0.53-0.82). The selected materials thus distinctly differ in weathering stage, clay and Fe-oxide content, and Fe-oxide crystallinity. The sequence of increasing weathering stage is DD < SR∼MO∼MB < EK < MU∼DJ.

11.3.2 Silicon adsorption in soils

FEF aliquots of soil materials from both sequences were in contact with the solution at ic = 1.1mM Si. The solution at ic = 0.6mM Si was used only for Mungo samples. In fixed conditions of pH, ionic force, temperature and solid:liquid ratio, the amount of Si adsorbed clearly depended on initial Si concentration (ic), contact time and soil type (Table 11.3). Whatever the ic value and the weathering sequence, Si concentration in solution decreased after 72h contact time, indicating a net Si adsorption in all soils, except in MO, where the concentration of Si increased at all contact times. In the Mungo sequence, after 72h contact time, relative Si depletion from solution was larger at ic = 1.18 mM (12-

Table 11.2: Iron content in fine earth (<2mm) and clay (<2μm) fractions: total iron content (Fe_t), DCB-extractable Fe content (Fe_d), and oxalate-extractable Fe content (Fe_o).

Prof.	Horiz.	Depth	Fraction<2mm			Fraction<2μm		
			Fe_t	Fe_d	Fe_o	Fe_t	Fe_d	Fe_o
			$g.kg^{-1}$					
DD	Ap	0-5	86.7	19.2	16.1	77.2	56.4	39.0
DD	AC	5-40	94.3	23.1	22.1	103.9	78.0	63.8
SR	Ap1	0-5	85.7	30.5	26.7	71.7	51.4	12.1
SR	Bw	21-33	113.5	40.3	38.2	101.9	78.2	49.8
MB	Ap	0-5	53.7	21.7	10.4	45.5	29.6	3.2
MB	AC	5-32	114.3	44.2	34.2	101.1	78.4	50.5
DJ	Ap1	0-5	114.6	69.1	19.4	123.0	98.5	25.7
DJ	Bt	15-66	140.7	85.1	25.0	132.2	101.1	31.0
DJ	Bw	66-115	127.3	81.9	20.1	127.1	96.4	24.2
MO	Ap2	5-20	91.7	33.5	15.7	61.9	40.0	22.9
MO	Bw1	20-60	104.1	36.0	20.9	70.5	40.1	21.1
MO	Bw2	60-92	118.6	34.7	18.8	79.9	45.8	24.2
EK	Ap2	5-32	116.1	47.2	26.7	80.1	55.3	31.8
EK	Bt	32-60	111.5	48.4	29.4	81.2	53.9	32.2
EK	Bw1	60-100	119.7	46.2	29.1	88.5	52.4	31.0
MU	Ap2	5-25	180.8	58.4	15.7	96.7	52.2	16.9
MU	Bt1	25-65	131.8	57.4	11.7	85.9	50.5	14.4
MU	Bt2	65-110	131.0	58.0	10.4	85.6	52.0	14.0

23%) than at ic = 0.61 mM (5-11%). At ic = 1.18 mM, Si depletion was larger for DJ (23%) than for DD (12%) after 72h, suggesting a positive impact of Fe-oxide content on Si adsorption. At other contact times, experimental data show a relative enrichment of Si in solution, at ic = 0.61 mM Si for DD, SR and MB and at ic = 1.18 mM Si for MO. These results suggest a supply of aqueous Si from mineral weathering and/or desorption of Si from mineral surface. In the Mt Cameroon sequence, Si depletion in solution was smaller than in Mungo soils: the maximum value amounted to 11% for EK against 23% for DJ.

The additional experiments carried out on DCB-treated FEF did not result in any Si adsorption by soils (not shown). Data from experiments performed on $SrCl_2$-washed FEF samples at ic = 1.18 mM (Table 11.4) show that for all soils, aqueous Si in solution progressively decreased with increasing contact time. Besides, at 72h contact time, Si depletion yielded to 23-33% in Mungo and 8-18% in Mt Cameroon soils, confirming that Si adsorption was larger in the former than in the latter.

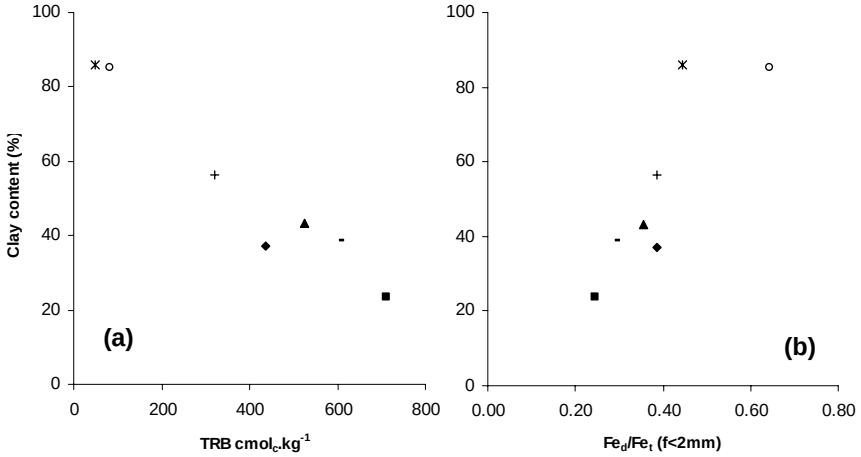

Figure 11.1: Plot of clay content against (a) total reserve in bases (TRB), and (b) Fe_d/Fe_t in the fine earth fraction (f<2mm) of the seven soil materials used for $H_4SiO_4^0$ adsorption experiment. DD = square, SR = triangle, MB = diamond, DJ = circle, MO = line, EK = cross, MU = star.

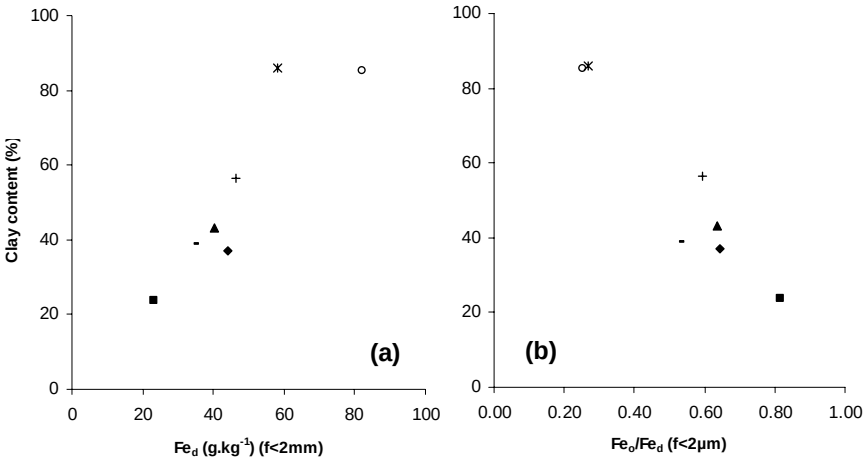

Figure 11.2: Plot of clay content against (a) Fe_d content in the fine earth fraction (f<2mm), and (b) Fe_o/Fe_t in the clay fraction ($<2\mu$m) of the seven soil materials used for $H_4SiO_4^0$ adsorption experiment. DD = square, SR = triangle, MB = diamond, DJ = circle, MO = dash, EK = cross, MU = star.

Table 11.3: Si concentration (mM Si) in solution as a function of contact time and soil material (FEF<2mm), for each initial Si concentration (time 0).

Horizon	0h	12h	24h	48h	72h
DD	0.61	0.62	0.61	0.58	0.56
SR	0.61	0.62	0.62	0.60	0.58
MB	0.61	0.63	0.62	0.58	0.56
DJ	0.61	0.61	0.59	0.57	0.54
DD	1.18	1.09	1.11	1.04	1.04
SR	1.18	1.11	1.10	1.01	0.95
MB	1.18	1.13	1.10	1.02	0.96
DJ	1.18	1.09	1.06	0.98	0.91
MO	1.18	1.19	1.22	1.22	1.25
EK	1.18	1.17	1.15	1.10	1.05
MU	1.18	1.15	1.13	1.11	1.08

Table 11.4: Si concentration (mM Si) in solution as a function of contact time and soil material (FEF<2mm) previously washed using $SrCl_2$, for initial Si concentration (time 0) at 1.18 mM Si.

Horizon	0h	12h	24h	48h	72h
DD	1.18	1.09	1.05	0.96	0.90
SR	1.18	1.09	1.02	0.88	0.79
MB	1.18	1.10	1.04	0.92	0.84
DJ	1.18	1.12	1.06	0.95	0.88
MO	1.18	1.13	1.12	1.09	1.08
EK	1.18	1.14	1.10	1.03	0.96
MU	1.18	1.13	1.11	1.10	1.08

11.3.3 Silicon isotopic fractionation during adsorption of monosilic acid

The δ^{30}Si values are reported as a function of contact time for the ic solutions 1.18 mM and 0.61 mM in Table 11.5. Measured against its initial composition ($\delta^{30}\text{Si} = +0.02 \pm 0.07‰$ ($\pm\ 2\sigma_{SD}$)), the solution was enriched in ^{30}Si, except for ic 1.18 mM Si in DD (24h) and MB (12h). After 72h contact time, the solutions were systematically enriched in ^{30}Si reaching maximum δ^{30}Si values ranging between +0.16‰ and +0.95‰, but with different sequences of increasing δ^{30}Si: DD < SR < MB <

DJ (0.61 mM Si); DD < SR < DJ < MB (1.18 mM Si); MO < MU <EK (1.18 mM Si). Whatever the sequence and the ic concentration, the lightest δ^{30}Si values were measured for the least weathered soils DD and MO. In the Mungo sequence, the heaviest δ^{30}Si values were measured for MB and DJ. In the Mt Cameroon sequence, the heaviest δ^{30}Si values occurred in EK. MO displayed a very peculiar trend as δ^{30}Si increased though Si concentration in solution increased. The whole set of δ^{30}Si values is illustrated in Figure 11.3, in which three populations of isotopic data (a, b, c) can be graphically distinguished with respect to the characteristics of the ic solutions whatever their Si concentration: δ^{30}Si = +0.02‰; fraction of Si left in solution (f) = 1.0.

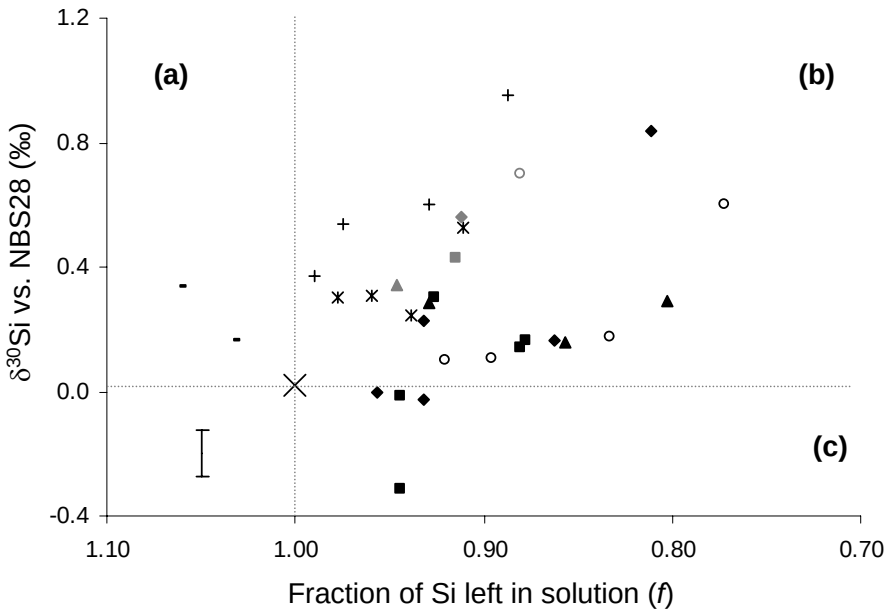

Figure 11.3: δ^{30}Si values (all measurements at various contact times, Table 11.5) plotted against the fraction of Si left in solution (f). The X refers to the initial solution whatever ic. Three zones are defined (see section 11.4.2): (a) mineral dissolution and Si adsorption, (b) Si adsorption, (c) Si desorption, for ic solutions 1.18 mM (black) and 0.6 mM Si (grey). DD = square, SR = triangle, MB = diamond, DJ = open circle, MO = dash, EK = cross, MU = star. The error bar corresponds to the $2\sigma_{SEM}$ (0.15‰) on single delta measurement.

Table 11.5: Isotopic compositions of the solutions (δ^{30}Si vs. NBS28 ± st error $2\sigma_{SEM}$ (‰)) as a function of contact time for the ic solutions 1.18 and 0.61 mM Si.

Solution mM Si	Horiz.	0h		12h		24h		48h		72h	
		δ^{30}Si	$2\sigma_{\mathrm{SEM}}$	δ^{30}Si	$2\sigma_{\mathrm{SEM}}$	δ^{30}Si	$2\sigma_{\mathrm{SEM}}$	δ^{30}Si	$2\sigma_{\mathrm{SEM}}$	δ^{30}Si	$2\sigma_{\mathrm{SEM}}$
0.61	DD	**+0.02**	0.07*	**-**	-	**-**	**-**	**-**	-	**0.43**	0.20
	SR	**-**	-	**-**	-	**-**	-	**-**	-	**0.34**	0.14
	MB	**-**	-	**-**	-	**-**	-	**-**	-	**0.56**	0.12
	DJ	**-**	-	**-**	-	**-**	-	**-**	-	**0.70**	0.19
1.18	DD	**-**	-	**+0.30**	0.12	**-0.16**	0.21*	**+0.14**	0.12	**+0.16**	0.11
	SR	**-**	-	**-**	-	**+0.28**	0.11	**+0.16**	0.10	**+0.29**	0.10
	MB	**-**	-	**+0.00**	0.12	**+0.10**	0.18*	**+0.17**	0.12	**+0.84**	0.13
	DJ	**-**	-	**+0.10**	0.11	**+0.11**	0.11	**+0.18**	0.09	**+0.60**	0.12
1.18	MO	**-**	-	**-**	-	**+0.17**	0.14	**-**	-	**+0.34**	0.11
	EK	**-**	-	**+0.37**	0.12	**+0.54**	0.14	**+0.60**	0.12	**+0.95**	0.11
	MU	**-**	-	**+0.30**	0.11	**+0.31**	0.12	**+0.24**	0.13	**+0.53**	0.10

* mean between two measurements each from different series (standard deviation $2\sigma_{\mathrm{SD}}$)

11.4 Discussion

11.4.1 Quantitative silicon adsorption and soil components

The dominant soil clay-sized minerals are secondary alumino-silicates (allophane, halloysite, kaolinite) and Fe-oxides (ferrihydrite, goethite) (Delvaux, 1988; Delvaux et al., 1989; Sieffermann, 1973). Minor quantities of gibbsite may occur in some soils. From the absence of any Si adsorption in DCB-treated soil samples, we deduce the crucial role of soils Fe-oxides in the quantitative adsorption of monosilicic acid. This is in very good agreement with the lack of Si adsorption observed onto allophane and kaolinite at pH 5.5 (Beckwith and Reeve, 1963; Wada and Inoue, 1974).

In Figure 11.4, we compare our adsorption data (Table 11.3) with the ones obtained in Chapter 10 for pure synthetic ferrihydrite and goethite in identical conditions of temperature, pH and ionic force, and using a similar solid:liquid ratio per Fe-oxide mass. Per solid mass, soil materials adsorbed less Si than synthetic oxides. At 72h

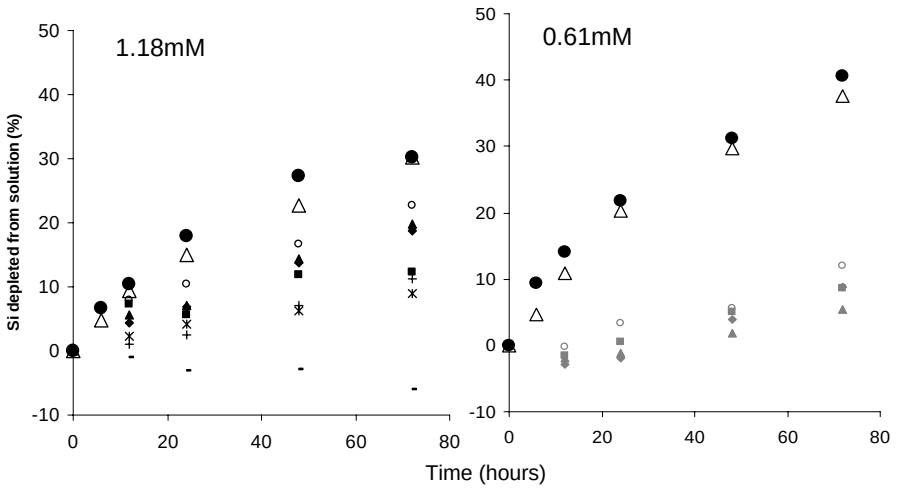

Figure 11.4: Proportion of Si depleted from solution as plotted against contact time for Si initial concentrations at 1.18mM (left) and 0.61 mM Si (right). Experimental data for synthetic ferrihydrite (large open triangle) and goethite (large black circle) are shown for comparison (Chapter 10). DD = square, SR = triangle, MB = diamond, DJ = open circle, MO = dash, EK = cross, MU = star.

contact time, for ic = 1.18 mM Si, maximum Si depletion in solution yielded around 20% for DJ (23%), SR (19%) and MB (18%) against 30% for pure synthetic ferrihydrite and goethite (Figure 11.4). Soils Fe-oxides were thus particularly reactive, despite that their surfaces were not cleaned up prior to adsorption. Soil Fe-oxide surfaces may have, indeed, previously interacted with $H_4SiO_4^0$, phosphate anions and organic matter (Borggaard, 1990; Guggenberger and Kaiser, 2003; Schwertmann and Taylor, 1989; Shoji et al., 1993; Sigg and Stumm, 1981). Si adsorption data from $SrCl_2$-washed samples (Table 11.4) support this interpretation, since Si depletion yielded up to 23-33% in Mungo and 8-18% in Mt Cameroon, against 11-23% and -6-11% for their respective untreated soil samples.

After 72h contact time at ic 0.61 mM Si, the aqueous Si concentration (0.54-0.58 mM) did not vary with Fe_d content (23-82 g kg^{-1}) (Tables 11.2 and 11.3). As illustrated in Figure 11.5 for ic = 1.18 mM Si, aqueous Si concentration progressively decreased with increasing Fe_d content in Mungo soils. The trend was, however, less clear in Mt Cameroon

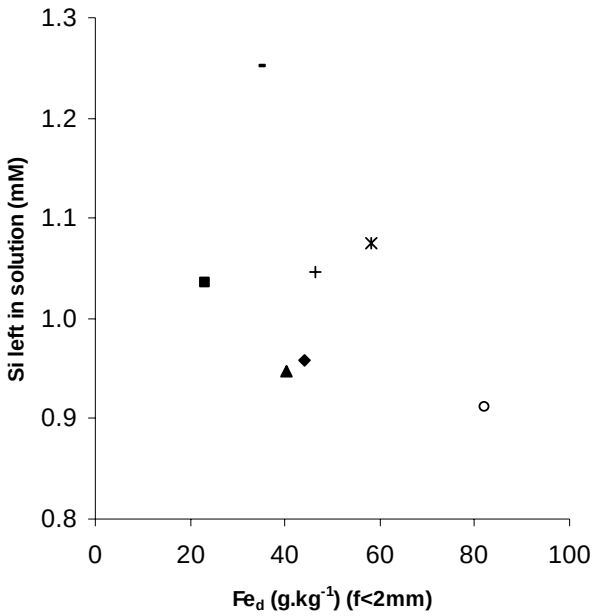

Figure 11.5: Si left in solution (bulk aqueous Si concentration) after 72h contact time vs. Fe_d content in FEF, at ic = 1.18mM. DD = square, SR = triangle, MB = diamond, DJ = open circle, MO = dash, EK = cross, MU = star.

soils, which adsorbed less Si at any Fe_d content. Since sro Fe-oxides adsorb more Si than crystalline Fe-oxides (Borggaard (1990); Jones and Handreck (1963); Chapter 10), the larger Si adsorption in Mungo soils could be related to their large proportions of sro Fe-oxides (Fe_o/Fe_d = 0.96, 0.95, 0.77, 0.25) relative to the ones in Mt Cameroon soils at similar weathering stage (Fe_o/Fe_d = 0.54, 0.63, 0.18). Within the Mungo sequence, the high Fe_d content (82 g kg^{-1}) likely explains the largest adsorption of Si in DJ. Within the Mt Cameroon sequence, EK (Fe_d = 46 g kg^{-1}; Fe_o/Fe_d = 0.63) adsorbed more Si than MU (Fe_d = 58 g kg^{-1}; Fe_o/Fe_d = 0.18). Considering the two weathering sequences, the quantitative adsorption of monosilicic acid is likely influenced by both the content and type of clay-sized Fe-oxides.

11.4.2 Isotopic fractionation during silicon adsorption as influenced by soil weathering stage

The enrichment in ^{30}Si in the solution provides evidence of a preferential adsorption of light Si isotopes onto soil Fe-oxides as shown on synthetic Fe-oxides (Chapter 10). The enrichment of light Si isotopes observed in soil clay fractions (Ziegler et al., 2005ab) may thus be partly controlled by Si adsorption onto secondary Fe-oxides.

Figure 11.6 illustrates the impact of Fe-oxide speciation on $\delta^{30}Si$ as measured at 72h contact time for both ic solutions. The $\delta^{30}Si$ enrichment in solution increased with the soil enrichment in Fe-oxides (Figure 11.6a), meaning that Si isotopic fractionation was closely linked with soil weathering stage. The trend was clear for most soil materials. However, EK and MB displayed the heaviest solution (Figure 11.6a), likely because of the dominant sro character of Fe-oxides in these soils (Figure 11.6b). Figure 11.6c where [Fe_d-Fe_o] estimates the content of crystalline Fe-oxide further suggests the grouping of two sets of data, whatever the ic: DD, MO, MU, DJ (r = 0.77) and DD, SR, MB, EK (r = 0.84). The slopes of these two sets of data significantly differ (0.06 and 0.43, respectively). Figure 11.6c first suggests that $\delta^{30}Si$ globally increases with increasing content of crystalline Fe-oxide. However, this increase is more important in soils rich in sro Fe-oxide (lower [Fe_d-Fe_o] content). These statements are in excellent agreement with recent data demonstrating that, relative to goethite, Si adsorption onto ferrihydrite induced a heavier Si signature in the residual solution (Chapter 10).

The Si isotopic fractionation globally increases with Si depletion in solution. However, different behaviors were deduced from adsorption data and $\delta^{30}Si$ values (Figure 11.3). Different soils with similar Si depletion showed very similar Si isotopic signatures in their residual

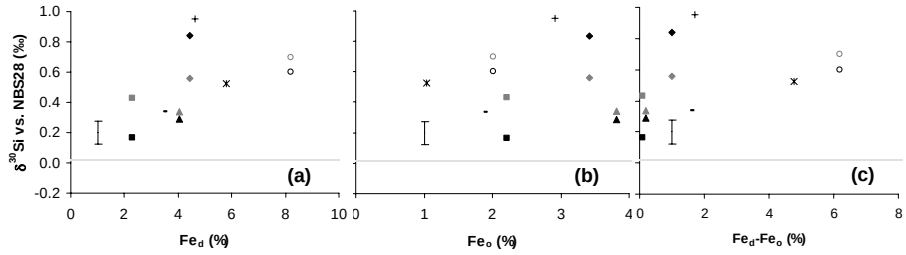

Figure 11.6: δ^{30}Si values in solution after 72h contact time vs.: (a) DCB-extractable Fe content (Fe_d), (b) oxalate-extractable Fe content (Fe_o), (c) estimated content of crystalline Fe-oxide (Fe_d-Fe_o) for ic solutions 1.18 mM (black) and 0.61 mM Si (grey). Dotted line: initial solution. DD = square, SR = triangle, MB = diamond, DJ = open circle, MO = dash, EK = cross, MU = star. The error bar corresponds to the $2\sigma_{SEM}$ (0.15‰) on single delta measurement.

solution (e.g. MB and SR after 48hours). For DD at ic = 1.18 mM Si, the concentration of Si left in solution was 1.09 mM at 12h and 1.11 mM at 24h (Table 11.3). This enrichment was coupled with a strong decrease of δ^{30}Si from 0.30 to -0.16 ‰ (Table 11.5), suggesting a release of light Si isotopes in solution, and thus likely a Si desorption from oxide surfaces, as supported by adsorption data from $SrCl_2$-treated samples (Table 11.4). For MO, the global Si enrichment in solution after 72h was parallel to an increase of Al, Fe, Ca, Mg and Na concentrations in solution (not shown), suggesting mineral dissolution, likely caused by the abundance of fine ash particle in these poorly developed soils (silt + clay content in MO = 65% against 39% in DD). Despite the Si release from mineral dissolution (measured in serie 1), the solution was depleted in light isotopes (measured in serie 2), indicating an adsorption process. However, isotopic balance calculation demonstrates that a heavier isotopic signature in solution after 72h can not be obtained if mineral dissolution is combined with Si adsorption (bulk soil close to primary minerals: -0.38 ‰, or lighter; Chapter 12). The mineral dissolution probably occured in serie 1 and not in serie 2. We thus suggest that three different processes likely interacted during the contact between FEF samples and ic solutions. They correspond graphically to the three areas distinguished in Figure 11.3 according to the values of δ^{30}Si and fraction of Si left in solution (f): (a) (δ^{30}Si $> +0.02$‰; $f > 1.0$) Si release in the solution results predominantly from mineral dissolution, but isotopic composition from Si adsorption; (b) (δ^{30}Si $> +0.02$‰;

$f < 1.0$) Si adsorption is dominant; (c) ($\delta^{30}Si < +0.2‰$; $f < 1.0$) the release of light Si isotopes results from Si desorption from oxide surface. The three processes interact so that the bulk Si isotopic signature of the solution should result from the dominant process. Any further interpretation of isotopic data would require evaluating the isotopic signature of the Si source available for Si adsorption (Appendix F).

11.4.3 Isotopic impact on soil solution and rivers

Our data provide unequivocal answers to the questions raised in the Introduction. (1) Si isotope fractionation readily occurs during Si adsorption onto soil Fe-oxides without any prior cleaning of oxide surface, privileging light Si isotopes and leaving a residual solution enriched in heavy ones. (2) Both Si adsorption and isotopic fractionation increase with increasing content of soil Fe-oxide and proportion of sro Fe-oxide in the global Fe-oxide pool. Thus soil weathering stage strongly influences Si adsorption and isotopic fractionation in the volcanic ash soils studied here through its impact on Fe-oxide content and type.

Our data further provide experimental evidence that the adsorption of monosilicic acid onto soil Fe-oxides can at least partly contribute to the sequestration of light Si isotopes in clay-sized fractions of soils and weathering profiles, and thus impact the isotopic signature of waters drained from soil environments. Rock weathering and soil development lead to the dissolution of primary minerals, formation of clay-sized silicates and secondary Fe- and Al-oxides. Mineral dissolution and clay synthesis leave pore waters enriched in ^{30}Si (Ziegler et al., 2005b). Pore waters from weathering profiles feed local streams at watershed level. The heavy Si isotopic riverine signature relative to that of crustal rocks (Douthitt, 1982) characterizes the hydrological output of silica (Georg et al., 2006a 2007c). In a humid tropical environment characterized by a large annual excess of precipitation over evapotranspiration (Delvaux, 1988), soil drainage would transfer to the hydrosystem pore waters affected by Si adsorption and clay formation, and thus enriched in ^{30}Si (Chapter 8). However, Si adsorption will be strongly limited if oxide surfaces are Si-saturated as shown experimentally with ^{32}Si (Ziegler et al., 2005a). Here, the weathering of Fe-rich primary minerals in basaltic ash soils led to the formation of Fe-oxide and thus oxide surfaces available for solute adsorption (Borggaard, 1990; Guggenberger and Kaiser, 2003; Sigg and Stumm, 1981). Weathered soil and saprolite layers thus acquired a high propensity to impact soil solutions and exported waters through Si adsorption. Although occurring at very different timescales (from the rainy event to the soil formation), the

processes of pore water drainage, clay-sized Fe-oxide formation and Si adsorption could impact the Si isotopic signal exported to oceans, as continental runoff water contributes to more than 80% of the Si input to the marine Si budget (Tréguer et al., 1995).

Silicon adsorption by soil Fe-oxides is thus a process which partly controls the heavier Si isotopic riverine signature transported to oceans, in addition to clay formation (Georg et al., 2006a 2007c; Ziegler et al., 2005b), Si uptake by plants (Ding et al. (2005b); Opfergelt et al. (2006b); Chapter 7) and diatoms (De La Rocha et al., 1997), and silica-rich inorganic precipitation (Basile-Doelsch et al., 2005).

11.5 Conclusions

Our data show that $H_4SiO_4^0$ adsorption by volcanic ash soils differing in weathering stage increased with both Fe-oxide content and relative proportion of short range ordered Fe-oxide (ferrihydrite). The adsorption process was parallel to an increase of δ^{30}Si values in the residual solution, meaning an enrichment of heavy Si isotopes in the solution. Thus both the quantitative Si adsorption and Si isotopic fractionation were influenced by the content and nature of Fe-oxides, both ruled by soil weathering stage.

We conclude that, in natural environments, Si adsorption could impact the isotopic signature of the pore waters exported to rivers.